Sensitivity of Alpine glaciers to anthropogenic atmospheric forcings: case study of the Argentière glacier

Léo Clauzel, Adrien Gilbert, Ménégoz Martin, Olivier Gagliardini, Delphine Six, Guillaume Gastineau

Sensitivity of Alpine glaciers to anthropogenic atmospheric forcings: case study of the Argentière glacier

Léo Clauzel[1], Adrien Gilbert[1], Martin Ménégoz[1], Olivier Gagliardini[1], Delphine Six[1], Guillaume Gastineau[2]

[1]Univ. Grenoble Alpes, CNRS, IRD, Grenoble INP, IGE, 38000 Grenoble, France

[2]UMR LOCEAN, Sorbonne Université/CNRS/IRD/MNHN, IPSL, 4 place Jussieu, 75005, Paris, France

Key points (140 character par key points, pas d'abréviation, 3 max)

- Ice flow simulations forced with climate model outputs are used to explore natural and anthropogenic imprints on the Argentière glacier.
- Statistical downscaling needs to ensure a conservation of the trends and the physical relationship between temperature and precipitation.
- The anthropogenic imprint on the Argentière glacier mass emerged from internal variability in 2003, 30 years after that on temperature.

Key words (6 max)

statistical adjustment - glacier modelling - external climate forcings - detection-attribution - time of emergence

Abstract (150 words < 150)

This study aims at quantifying the contribution of external climate forcings on the retreat of the Argentière glacier (Mont-Blanc area). Its evolution is simulated over 1850-2014 following retrospective scenarios produced with the IPSL-CM6-LR climate model, excluding and including natural and anthropogenic forcings. These scenarios are statistically adjusted at the local scale, ensuring a preservation of the long-term trends and a physical consistency between precipitation and temperature, to finally force an ice flow model coupled with a surface mass balance scheme. The regional aerosol cooling partly counteracted the greenhouse gases warming, delaying the time of emergence of anthropogenic signals: The anthropogenic influences emerged from the natural variability in 1979 for temperature and in 2008 for the mass of the glacier, whereas its snout position in 2014 remains compatible with natural variability. We found that 66% [20-112%] of the total mass loss in 2014 since 1850 can be attributed to anthropogenic activities.

Plain Language Summary (200 words max sans acronymes)

This work aims at quantifying the anthropogenic imprint on the Argentière glacier with respect to its changes related to climate natural variability. It is based on a detection-attribution approach used to produce retrospective ensemble simulations of the climate and the glaciers, including and excluding greenhouse gases and aerosol forcings over 1850-2014. The time of emergence of the anthropogenic signal, i.e. the date when it becomes statistically incompatible with climate internal variability, occurs in 1979 for temperature in the Argentière location, with a warming reaching 1.35 °C in 2014. It occurs later for the glacier changes, in particular for

the snout position that is still compatible with internal variability in 2014. For the glacier mass, it occurred in 2008, ~30 years after those of the temperature. In 2014, 66% [20-112%] of the total mass loss since 1850 can be attributed to anthropogenic activities. This result is sensitive to the internal variability estimate from the climate model, and it should be completed in further studies including both the cooling of the aerosols when they are located in the atmosphere and the melt increase when they are deposited onto the snow. This study highlights a strengthening of the current glacier retreat.

1. Introduction

Mountain glaciers around the world retreated dramatically over the last decades. Appart being an iconic symbol of the ongoing climate change, this retreat has strong environmental and societal impacts: over 1971-2018, the mass loss of mountain glaciers is the second contributor to sea level rise, with a 22% contribution, coming after the 50% related to the thermal expansion of the ocean and before the 20% explained by the ice caps melting (IPCC, 2021). The retreat of glaciers is also a threat for water availability in particular where they play the role of fresh water reservoirs essential for biodiversity and human societies (Kaser et al., 2010; Milner et al., 2017; Laurent et al., 2020).

Alpine glacier extensions reached a maxima at the end of the little ice age (LIA; Zumbühl and Nussbaumer, 2018). The LIA covers approximately 1400-1700, a cold period induced by strong volcanic activity and a minimum of solar activity (Mann et al., 2009). After the LIA, the 18th century is considered as a temperature constant reference period without any strong external forcing (Hawkins et al., 2017), whereas low temperature has been observed again during the period 1800-1850, in relation to volcanic eruptions and changes of solar activity that favoured large glacier extensions in the Alps (Zumbühl and Nussbaumer, 2018). The retreat of Alpine glaciers started in 1850, simultaneously with the beginning of anthropogenic emissions of greenhouse gases (GHGs). The exact causes of this retreat are still debated, since the temperature increase was relatively small during the end of the XIXth century, and other factors like decadal variability of precipitation (Vincent et al., 2005) and deposition of absorbing aerosols on snow (Painter et al., 2013) might have also affected glaciers. Future glacier projections need to be considered carefully because the glacier sensitivity to external forcing and climate internal variability is still uncertain (Marzeion et al, 2020).

Detection-attribution studies have been used to estimate the climate response to external forcings, using both climate models and observations of surface air temperature. Such studies typically estimate that the global warming of +1.2°C (+/-0.15°C), observed in 2010-2020 as compared to the pre-industrial era, can be decomposed in +1.5°C (+/-0.3°C) related to GHGs and -0.4°C (+/-0.3°C) related to other forcings (Haustein et al., 2017 ; Gillett et al., 2021 ; Ribes et al., 2021 ; Eyring et al. 2021). These other forcings mainly reflect the effect of anthropogenic aerosols that cool the atmosphere. Detection-attribution methods allow to highlight the climate response to external forcings with respect to internal variability. Following such an approach, Roe et al. (2017; 2021) suggested that 100% of the glacier global mass loss from the pre-industrial era is explained by anthropogenic forcings. However, such approaches do not allow to accurately quantify the emergence of the anthropogenic signals at the local scale and cannot be used to differentiate the role of GHGs and aerosols, because they are based on idealised depictions of the climate and the glacier systems. More physical approaches are

used to quantify separately the natural and anthropogenic imprints on glaciers with global models (e.g. Marzeion et al., 2014; Maussion et al., 2019) and their contribution to sea level changes (e.g. Huss and Hock, 2015). These approaches are inevitably strongly idealised for global applications, in particular because of the complexity of the physical processes at play that cannot be verified due to the impossibility to get observational data for all the glaciers on the Earth. To be fully reliable, physical approaches would require: (1) a realistic atmospheric forcing, that is generally obtained from the statistical adjustment of atmosphere-ocean general circulation models (AOGCMs) outputs, used to extrapolate the local observations when they are not available. Several adjustment techniques has been proposed to ensure a conservation of the trends and the interannual variability of atmospheric variables, as well as a physical consistency between themselves (Latombe et al., 2018; Luo et al., 2018, Gutierrez et al., 2019, Vaittinada et al., 2021); (2) a model allowing to simulate the 3D glacier flow and its geometry evolution, that needs local observations for calibration; (3) an adequate initialisation of the glacier model, a crucial step since climate internal variability might induce strong decadal variations of glaciers, even in a non-perturbed climate.

The aim of this study is to investigate the drivers of the Argentière glacier changes in the Alpine area over 1850-2014 by quantifying separately the impacts of GHGs, aerosols and climate internal variability. After a presentation of the data and the methods in Section 2, the results are described in Section 3, before a discussion and a conclusion in Section 4.

2. Data and Methods

2.1 Local observations and climate forcing

Located in the Mont-Blanc massif, the Argentière Glacier (45°57'N, 6°58'E) is the second largest glacier in the French Alps, covering an area of 11.3 km² in 2019, extended over ~10km from 1550 to 3500 m a.s.l. (Six and Vincent, 2014). Stake measurements, geodetic observations, GPS survey and radar observations (Rabatel et al., 2018; Vincent et al, 2009) are used to monitor this glacier within the framework of the GLACIOCLIM observatory (https://glacioclim.osug.fr/).

Atmospheric data is extracted here from experiments produced with the IPSL-CM6A-LR AOGCM (Boucher et al., 2020), in the context of the Detection and Attribution Model Intercomparison Project (DAMIP, Gillett et al., 2016) panel of CMIP6 (Coupled Model Intercomparison Phase 6). DAMIP aims at quantifying separately the imprint of natural and anthropogenic external climate forcing. We use here a subset of the IPSL-CM6A-LR experiments: (i) a 10-member historical experiment (*hist*) that includes all natural and anthropogenic forcings and 3 sets of 6-member experiments, including (ii) only the natural (*nat*), only the anthropogenic aerosol (*aer*) and only the anthropogenic greenhouse gas (*ghg*) forcings. The *hist* simulations also include the effect of changing stratospheric ozone and land use, but these two effects should only play a minor role at the local scale in the Mont-Blanc area. The natural external forcings designate here the volcanic and the solar activities. The simulations are available over 1850-2014 and member-experiments differ between themselves only by their initial conditions that have been sampled from a 1000-year pre-industrial control experiment. Corresponding members from one experiment to another one have the same initial conditions. Hereafter, the internal variability designates the variability

sampled with the different ensemble members. The SAFRAN reanalysis available for the different French Alpine regions with a 300m vertical resolution (Vernay et al., 2022) is used here to statistically adjust the AOGCM data extracted from the gridpoint containing the Argentière Glacier.

2.2 Statistical downscaling of climate data

The daily AOGCM temperature and precipitation are simultaneously bias corrected and downscaled with a monthly statistical adjustment, considering the difference between the *hist* experiment and the SAFRAN reference at 2400m a.s.l., i.e. close to the glacier mean altitude. The adjustment is calibrated over 1975-2014 with the 10 *hist* members and is then applied to the whole set of ensemble experiments hist, *nat*, *aer* and *ghg,* considering the correction stationary over 1850-2014.

The simple quantile mapping (SQM, Panofsky and Brier, 1968) is used here to fit the cumulative distributive function of the model variables on the observation ones. However, this method induces a spurious amplification of the long term temperature trend (Figure 1a) and an underestimation of snow accumulation as the precipitation distribution over the temperature 1°C-width bins is shifted to warmer days (Figure 1b). To overcome these issues, the Quantile Delta Mapping (QDM, Cannon et al., 2015), that ensures a conservation of trends, is first used to adjust temperature. The 2D-variable successive conditional approach of Piani and Haerter (2012) is then followed by applying the SQM methods for precipitation separately for 5 quantiles of temperature, to keep the physical consistency between the two variables. The temperature-quantile bins are defined on 40-year moving sub-periods to avoid any impact of temperature trends on the precipitation adjustment. This combination of these two statistical adjustments is defined here as the Coupled Delta Quantile Mapping (CDQM).

The CDQM method ensures a conservation of the temperature trend simulated with the AOGCM that is in accordance with the HISTALP reconstruction (Böhm et al., 2010; Figure 1a), a physical precipitation-temperature relationship consistent with the SAFRAN reanalysis (Figure 1b) as well as realistic seasonal cycles, daily and interannual variability for these two variables (Figure S1).

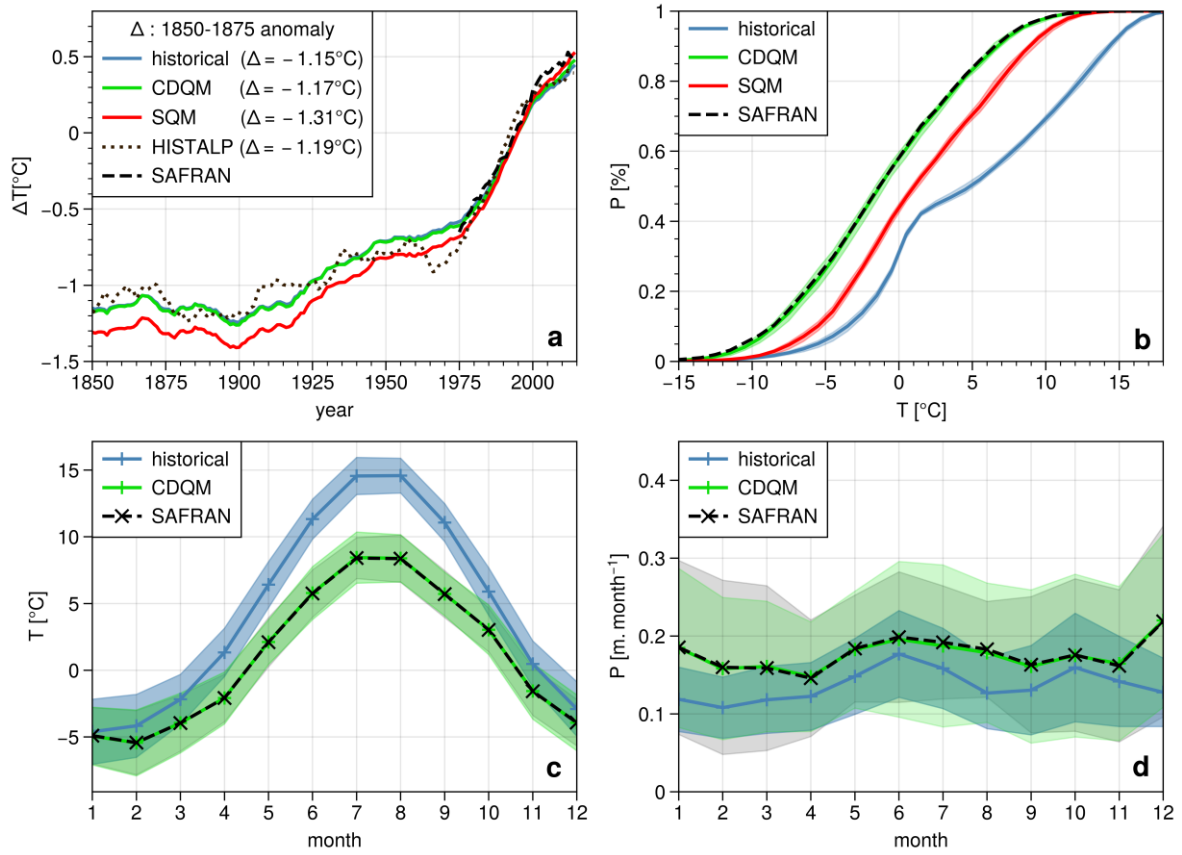

Figure 1. (a) 30-year running mean temperature anomaly with respect to the 1975-2014 mean, averaged over members. Blue line is the historical simulations, red and green lines are respectively their SQM and CDQM adjustments. The HISTALP data is denoted with the black dotted line and SAFRAN with the dashed line. The Δ given in brackets is the difference between the 1850-1875 and the 1975-2014 means; (b) cumulative distribution function of precipitation over 1°C-wide bins of temperature, averaged over members ; (c) cumulated SMB and (d) length change from 1850. Dashed lines are individual members and solid lines are the 10-member mean in (cd). The glaciological simulation forced with SAFRAN corresponds to the black line, the GLACIOCLIM in-situ data appears in brown, the estimate from Zemp et al. (2019) in cyan, geodetic data are denoted with blue crosses and proxies with the black points. Proxies are derived from moraine isotopic analysis (Protin et al., 2019).

2.3 Glaciological model

2.3.1 Ice flow model

The glacier response to climate forcing is simulated using a coupled surface mass balance - 3D ice flow model based on the Elmer/Ice finite element code (Gagliardini et al., 2013). The ice flow model solves the Stokes equations adopting Glen's flow law for viscous isotropic temperate ice (Cuffey & Paterson, 2010). The basal boundary condition is given by a Weertman-type friction law (Weertman, 1957):

$$A_s {\tau_b}^m = u_b \quad (1)$$

where τ_b is the basal shear stress (*MPa*), u_b the sliding velocity (*m yr*$^{-1}$), A_s the friction coefficient (*m yr*$^{-1}$ *MPa*$^{-m}$) and *m* an exponent fixed to $m = 3$ for Argentière glacier (Gimbert et al., 2021). The friction coefficient A_s is assumed to be uniform and constant in time. The evolution of the ice thickness is computed at a 1/20 year time step (~18 days) through the

resolution of the free surface equation for the given surface mass balance and ice velocity field (Gagliardini et al., 2013).

2.3.2 Surface Mass Balance scheme

The mass balance scheme computes the daily distributed surface mass balance (SMB) from daily precipitation and temperature which is then cumulated over the 1/20 year simulation timestep to force the ice flow model. The local net daily SMB (m w.eq. d^{-1}) is determined by:

$$SMB = A - M \quad (2)$$

where *A* and M are respectively the local daily snow accumulation and surface melting ($m\, w_{eq}\, d^{-1}$). The amount of melt *M* is computed from the available energy for melt following Oerlemans (2001):

$$Q_m = (1-\alpha) r I_{pot} + k_1 T + k_0 \quad (3)$$

where α is the local surface albedo, I_{pot} is the potential incoming short-wave radiation (Hock, 1999), *r* a corrective factor and $k_1 T + k_0$ is the sum of the long-wave radiation balance and the turbulent heat exchange linearized around the melting point with k_0 and k_1 as constant parameters, and T the air temperature. If Q_m is positive, the melt rate is obtained with the latent heat of fusion *L*:

$$M = Q_m / (L \times \rho_{water}) \quad (4)$$

The local surface albedo is estimated from the state of the surface that can be either snow or ice. Snow and firn thickness evolution is computed at daily time step to determine if $\alpha = \alpha_{ice}$ or $\alpha = \alpha_{snow}$ (Gilbert et al., 2020). The local snow accumulation *A* is determined from local daily precipitation according to a snow/rain temperature threshold fixed to 1°C.

Temperature and precipitation data provided at 2400m are distributed to the glacier surface according to altitudinal lapse rates such as:

$$T(z,t) = T_{ref}(t) + \frac{dT}{dz}\left(z - z_{ref}\right) \quad (5)$$

$$P(x,y,z,t) = M_a(x,y)\, P_{ref}(t)\, \left(1 + P_z\left(z - z_{ref}\right)\right) \quad (6)$$

where *z* is the elevation of the surface (*m*), $T_{ref}(t)$ and $P_{ref}(t)$ are air temperature (°C) and precipitation (m w.eq.) at the elevation $z_{ref} = 2400m$, $\frac{dT}{dz}$ is the temperature lapse rate (°C m^{-1}), P_z is the precipitation lapse rate and $M_a(x,y)$ is a spatial correction factor for precipitation (Table S1).

2.4 Modelling strategy

2.4.1 Model calibration

In-situ stake measurement of seasonal mass balance performed since 1975 combined to SAFRAN temperature and precipitation are used to constrain the SMB scheme. The extensive monitoring of the glacier over a long period allowed a good calibration of the multiple

parameters. The SMB scheme is calibrated on a fixed surface topography (1998) such that the ice flow model is not needed for this step. We verify a posteriori that the SMB remains in good accordance with the observations when the model is coupled with the ice flow model. Precipitation correction factor and lapse rate were first calibrated using winter SMB data in which little melting happened. The observed SMB altitude dependency strongly constraints k_1, α_{ice} and α_{snow} whereas the total mass change over the whole measurement period constraints *r* and k_0. The adopted model parameters values are summarised in Table S1.

2.4.2 Initial state and spin up

The 1820 steady-state glacier geometry is obtained by running the SMB scheme coupled to the ice flow model forced with the 1975-2015 SAFRAN data, assuming a shift of temperature $\mathbf{\Delta}T_0$ and supposing unchanged precipitation rates. A value of -1.30°C for $\mathbf{\Delta}T_0$ is required to obtain a glacier length that matches the 1820 moraine observation, a period when the glacier was supposed to be in equilibrium with the climate for several decades (Protin et al., 2019). A 30-year spin up over 1820-1850 is then performed separately for the 10 members, allowing to adjust the glacier shape to the climate internal variability that might induce large interannual to decadal changes of temperature and precipitation. These spin-ups are forced with the statistically adjusted atmospheric data produced in the DAMIP spin-up experiments themselves, covering the same period.

3. Results

3.1 Observed versus simulated glacier changes

By construction, there is a good consistency between the SMB estimated from stakes observations and those simulated with the SAFRAN data over the reference period 1975-2014, both in terms of mean and trends (Figure S2). The interannual variability of the SMB is slightly overestimated in the adjusted model (Figures S2). The ensemble mean of the experiment is close to the observed SMB. The cumulative SMB shows stabilised values during the 1970's followed by a dramatic retreat from the middle of the 1980's that reached a cumulated change of -35m.w.eq. (Fig. 1c) and a length change of -1700m in 2014 (Fig. 1d) as compared to the 1850 levels. The consistency between the model and the observations before 1975 demonstrates that the glaciological model is able to accurately simulate both the SMB and the glacier flow (Figure 1c,1d). This also confirms the realism of the adjusted AOGCMs outputs applied to the glaciological model. The large spread in the ensemble members suggests that internal climate variability can induce large low-frequency variations of the glacier mass and length (Figure 1c,1d). This might reflect the large centennial variability simulated in this model (Jiang et al. 2021).

3.2 Pre-industrial conditions

The experiments are spinuped from an initial steady state imposed by the 1820 moraine, that can be simulated with a temperature decrease $\mathbf{\Delta}T0$=-1.30°C (Section 2.4.2). This $\mathbf{\Delta}T0$ is close to, albeit slightly cooler, the $\mathbf{\Delta}T$ estimated from the AOGCM outputs that reached -1.15°C in the 10-member historical experiment and -1.17°C in the corresponding adjusted values (CDQM, Figure 1a). This slight difference explains that even with constant forcing levels during 1820-1850 (Figure 2ab), there is a negative trend of SMB for all the members during this spin up period (Figure 2c). This negative trend is visible in the different positions of the glacier front

in Figure 3a, where all the members show a retreat, with a spread centred on the 1850 position. This spread highlights the different positions that could have reached the glacier front with stable external forcings during this 30-year period.

3.3 Forced versus climate internally driven signals

For a strict comparison with the 6-member DAMIP IPSL experiments ghg, aer and nat, only the 6 corresponding members are retained in hist, as shown in Figures 2 and 3. Figure 2a highlights the local warming simulated at the Argentière Glacier in hist, starting in 1850, intensifying in the 1980's and reaching +1.42°C in 2014. This warming is mainly related to GHGs as evidenced in ghg (+1.56°C) and is partly compensated by the cooling effect of anthropogenic aerosols, as evidenced in aer (-0.74°C). The warming found in hist does not reach exactly aer+ghg+nat. Precipitation rates are stable and similar in all the experiments, suggesting a minor impact of external forcings on this variable, except in ghg for which precipitation is slightly strengthened and in aer for which precipitation is slightly decreased. Although the temperature increase due to GHGs is twice larger than the decrease due to aerosols, the GHGs and aerosols effects on precipitation nearly cancel each other. These precipitation changes are related to the radiative changes driven by greenhouse gases and aerosols, as well as potential atmospheric circulation changes (Myrhe et al. 2017). The resulting precipitation rates remain nearly unchanged in both hist and nat.

The cumulated SMBs show larger member spread as compared to those of temperature in all the experiments, highlighting a large imprint of climate internal variability on SMB (Figure 2c). As for temperature, the cumulated SMB simulated in 2014 under hist (~ -45m.weq) is explained by the combined but no-additive trends found in aer (~ -5m.weq), nat (~ -22m.weq) and in ghg (~ -60m.weq). SMB is decreasing in all the experiments, even in nat (~ -22m.weq). This suggests that the glacier retreat that would have occurred even without any anthropogenic forcing is related to the end of the LIA. The interannual variability of SMB is relatively high in both the observations and the model (Figure 2d), and positive values never occurred in the observations after the 2000's. The spread of the ensemble experiment is larger for the glacier length than for the SMB (Figure 2), probably explained by non-linear dynamical processes. According to geomorphologic observations (Leclercq et al., 2014), the position of the Argentière Glacier front varied between -800m and 0m over 1600-1820, reaching its maximum in 1820 (Figure 2e). In 2014, it reached -2000m in the observations, a pattern reproduced in the hist configuration that corresponds to an equilibrium between the ghg (-2800m), the nat (-1000m) and the aer (-300m) configurations.

The time of emergence is defined here as the time at which the signal of climate change emerges from the noise of natural climate variability (Hawkins and Sutton, 2012; IPCC, 2021). Here, it is estimated by computing annually the probability that the glacier is bigger than those simulated in the nat experiment after a 1000-time bootstrap resampling over the members. The vertical bars in Figure 2abcef highlight the date when this probability is very unlikely ($P<0.1$). In the ghg experiment, the time of emergence occurs in 2001 for the glacier length, in 1987 for SMB and in 1970 for temperature(orange vertical bars in Figure 2ace). The anthropogenic signal has not emerged significantly before 2014 in the hist configuration ($P=0.13$), whereas it emerged in 2008 for SMB and in 1979 for temperature (blue vertical bars in Figure 2ace).

The ensemble mean of glacier extents is shown in Figure 3b: the hist configuration leads to an extent close to the 2014 observation; the nat configuration suggests a glacier retreat less pronounced than in the hist one; the aer configuration induces a growing of the glacier that comes back to the levels observed during the middle of the 19th century, and the ghg configuration leads to a retreat more pronounced than the hist one. The spatial impact of climate internal variability on the extent of the Argentière Glacier is depicted for the four sensitivity experiments in Figure 3abcd. Most of the hist members are concentrated close to the 2014 observation except one that retreated more. The nat ensemble shows a large spread, with members extending from the 1850 moraine to areas located at higher elevation than the 2014 observation. The entire ghg ensemble show extensions located at higher elevation than the 2014 observation, whereas all the members of the aer ensemble extend until the bottom of the valley, around the LIA moraines.

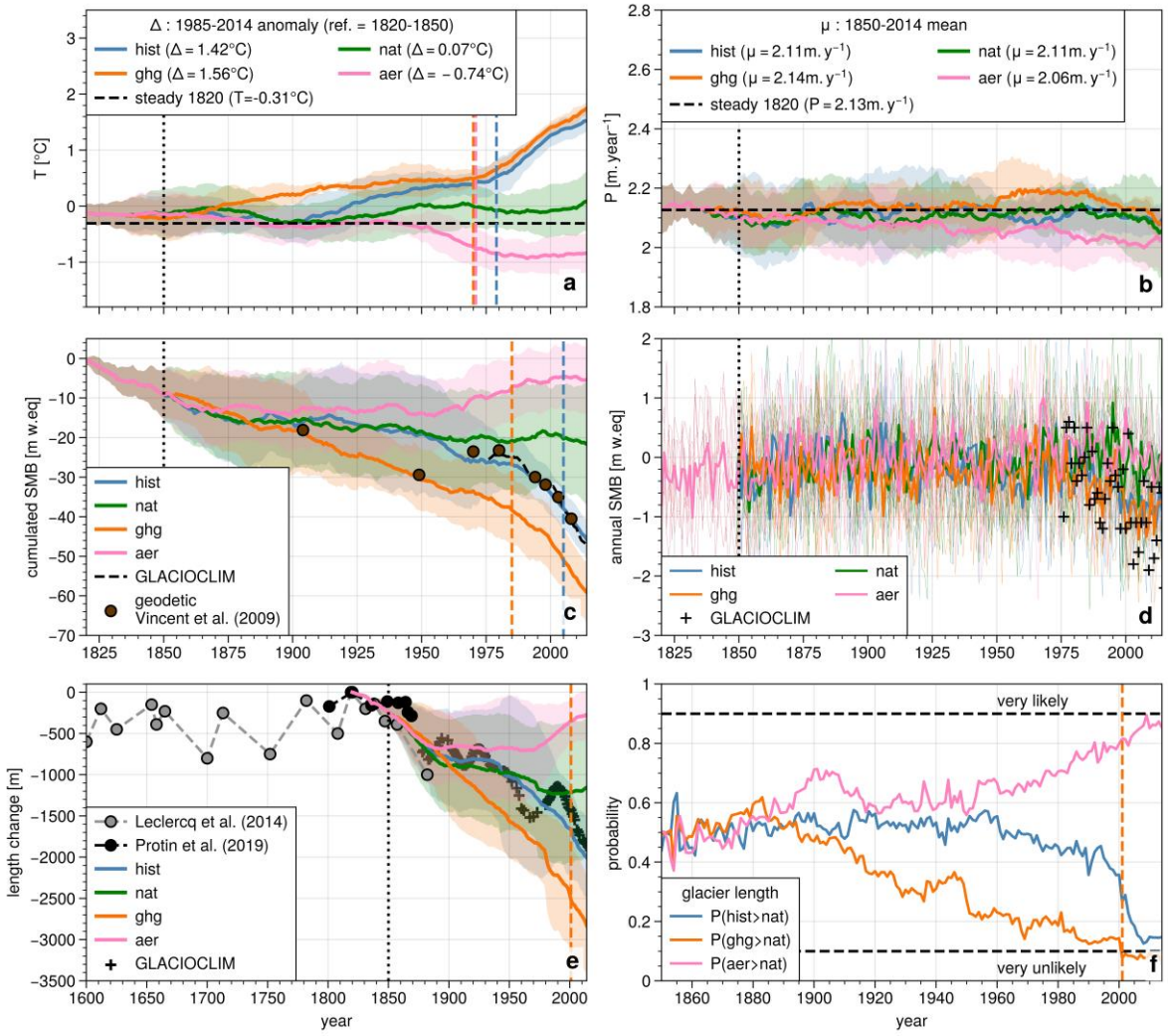

Figure 2. 30-year running mean of (a) adjusted temperature and (b) adjusted precipitation ; (c) cumulated SMB from 1820 ; (d) annual SMB ; (e) length change from 1820 and (f) empirical probability of having a larger glacier length than *nat* computed by comparing experiment distributions based on 1000-time bootstrap resampling. Solid lines are 6-

member means, shading corresponds to the 1-σ member range, vertical black lines show the spin up end. Vertical coloured dashed lines indicate the year by which it is very likely or very unlikely to have a higher temperature or a lower value for SMB and glacier length than in *nat* as computed in (f). Steady 1820 in (a) and (b) refers to the mean climate conditions used for constructing the 1820 steady state.

331

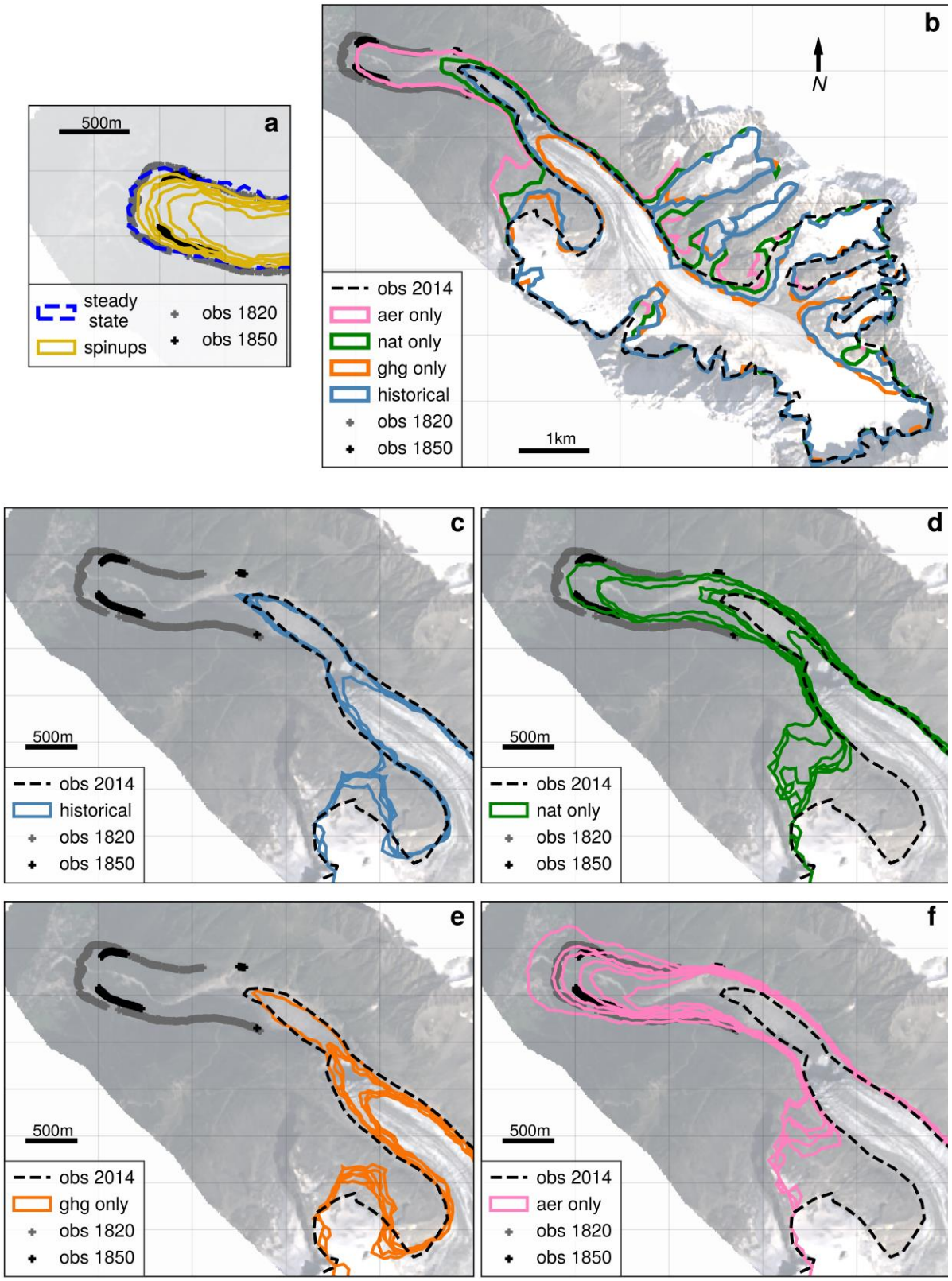

Figure 3. (a) Glacier extent observed in 1820 and 1850 and simulated under pre-industrial climate conditions after a 30-year spinup experiment. (b) 6-member mean of the whole glacier area for the different experiments in 2014 and their corresponding individual members in the front area in (c) *hist*, (d) *nat*, (e) *ghg* and (f) *aer*. The black dashed line is

the observed glacier extent in 2014.

4. Discussion and conclusions

The time of emergence of anthropogenic signals in the Argentière Glacier has been investigated using the adjusted IPSL-CM6 AOGCM to force an ice-flow model coupled with a SMB scheme. The effects of GHGs, anthropogenic aerosols and natural forcings are disentangled using dedicated detection-attribution AOGCM runs. The unavoidable adjustment required to bias-correct and downscale the AOGCM outputs to the local scale needs to be considered with caution. Here, we use a method that preserves the temperature trends from the climate model as well as the physical consistency between temperature and precipitation. Other simple statistical adjustment might result in spurious trends and erroneous accumulation rates.

The temperature change simulated with the AOGCM over 1850-2014 (-1.19°C) is similar to those found in HISTALP (-1.17°C) and the glacier length simulated in 1820-1850 is consistent with the morain observations. This gives credence in our modelling strategy, demonstrating that: (i) the 1850 glacier extension was an extreme state in the pre-industrial climate conditions, reached at the end of the LIA and (ii) a part of the retreat of the Argentière Glacier would have likely occurred even without any anthropogenic forcing. When excluding anthropogenic forcing, the more likely extension would have been located at an intermediate elevation between the 1850 and 2014 positions (Figure 3d). However, both the 1850 extension and positions higher than those observed in 2014 are compatible with natural variability over this period. This result is dependent on the strong multidecadal internal variability simulated in the IPSL-CM6-LR (Parsons et al., 2020). Ensemble spreads are larger in nat than in hist and ghg, suggesting that GHGs anthropogenic forcings reduced the interannual to interdecadal variability of temperature, SMB and glacier lengths over the last decades in the Alps, a hypothesis demonstrated at the global scale for the IPSL-CM6-LR model in Bonnet et al. (2021).

By comparing the hist and the nat experiments, the cumulative mass loss of the Argentière glacier due to anthropogenic forcing over 1850-2014 is estimated to 66% [20-112%]. This local estimation is lower than the global estimate of Roe et al. (2021), ranging between 85% and 180%, and higher than those reported by Marzeion et al. (2014), reaching 25%. Using a physical approach highly constrained by observations, we assume that the uncertainty provided here is mainly the result of climate internal variability whereas global estimates do not disentangle internal variability from model uncertainties. The similar evolution of the Argentière glacier as compared to the other Alpine glaciers over the previous centuries (Figure 1c) suggests that its response to anthropogenic forcings provide a general view of the glacier changes in the Alps.

Overall, the length of glaciers is an interesting proxy of the decadal to centennial climate variability, because it is easy to observe and acts as climate integrators, smoothing the variability of the atmosphere at higher frequencies. Conversely, glacier lengths show a larger spread of response to climate internal variability as compared to temperature and SMB. Indeed, the front position is largely influenced by the local topographic conditions such as valley shape and slope distribution. Applying such a physical model chain allows to accurately simulate the glacier length dependency to complex terrain. The next step in the ice-flow model development concerns the basal sliding related to subglacial hydrological processes that could further enhance the spread of member experiments for glacier length.

The warming simulated in hist in the Mont-Blanc area does not reach the sum of the aer, ghg and nat temperature signals. The land use or stratospheric ozone that are not considered separately here could drive changes of local temperature, but these ones are expected to be small (Eyring et al. 2021). We suggest that this non-additivity results from nonlinear processes related to local feedbacks, atmospheric circulation changes and residual internal climate variability. In addition, further research using a multi-model DAMIP approach would allow a better estimation of uncertainty, since climate signals, regional circulation changes and internal variability can vary widely from one AOGCM to another one (Myrhe et al. 2017). Finally, these experiments should be repeated in further study taking into account both the cooling effect of atmospheric aerosols and the melt increase related to the deposition of absorbing aerosols, a process known for its strong impact on the cryosphere (Reveillet et al., in press) that has been neglected here. This would allow to quantify exactly the contributions of all the external forcings that affected the cryosphere from the beginning of the industrial era.

5. Acknowledgment

The CMIP6 project at IPSL used the HPC resources of TGCC under the allocations 2016-A0030107732, 2017-R0040110492 and 2018-R0040110492 (project gencmip6) provided by GENCI (Grand Équipement National de Calcul Intensif). This study benefited from the ESPRI (Ensemble de Services Pour la Recherche à l'IPSL) computing and data center (https://mesocentre.ipsl.fr) which is supported by CNRS, Sorbonne Université, École Polytechnique and CNES and through national and international grants. All the glaciological simulations presented in this paper were performed using the GRICAD infrastructure (https://gricad.univ- grenoble-alpes.fr), which is supported by Grenoble research communities. This work is supported by the French ANR project SAUSSURE (ANR-18-CE01-0015-01).

6. Open research

Observational data from GLACIOCLIM observatory are available at the following link : https://glacioclim.osug.fr/.

CMIP6 and DAMIP data is available on the Earth System Grid Federation (ESGF, https://esgf.llnl.gov/).

The modelling code is based on the open-source code Elmer/Ice available at http://elmerice.elmerfem.org/wiki/doku.php

The glacier meshing file, the glaciological model configurations, the datasets generated and analyzed and the python jupyter notebook used in the current study are available on the repository platform Zenodo at the following link : https://zenodo.org/deposit/6786833 (to be published soon)

7. References

Allan, R.P., Cassou, C., Chen, D., Cherchi, A., Connors, L., Doblas-Reyes, F.J., Douville, H., Driouech, F., Edwards, T.L., Fischer, E., Flato, G.M., Forster, P., AchutaRao, K.M., Adhikary, B., Aldrian, E., Armour, K., n.d. IPCC, 2021 : Summary for Policymakers 32.

Böhm, R., Jones, P.D., Hiebl, J., Frank, D., Brunetti, M., Maugeri, M., 2010. The early instrumental warm-bias: a solution for long central European temperature series

1760–2007. Climatic Change 101, 41–67. https://doi.org/10.1007/s10584-009-9649-4

Bonnet, R., Boucher, O., Deshayes, J., Gastineau, G., Hourdin, F., Mignot, J., Servonnat, J., Swingedouw, D., 2021. Presentation and Evaluation of the IPSL-CM6A-LR Ensemble of Extended Historical Simulations. Journal of Advances in Modeling Earth Systems 13, e2021MS002565. https://doi.org/10.1029/2021MS002565

Boucher, O., Servonnat, J., Albright, A.L., Aumont, O., Balkanski, Y., Bastrikov, V., Bekki, S., Bonnet, R., Bony, S., Bopp, L., Braconnot, P., Brockmann, P., Cadule, P., Caubel, A., Cheruy, F., Codron, F., Cozic, A., Cugnet, D., D'Andrea, F., Davini, P., de Lavergne, C., Denvil, S., Deshayes, J., Devilliers, M., Ducharne, A., Dufresne, J.-L., Dupont, E., Éthé, C., Fairhead, L., Falletti, L., Flavoni, S., Foujols, M.-A., Gardoll, S., Gastineau, G., Ghattas, J., Grandpeix, J.-Y., Guenet, B., Guez, E., Lionel, Guilyardi, E., Guimberteau, M., Hauglustaine, D., Hourdin, F., Idelkadi, A., Joussaume, S., Kageyama, M., Khodri, M., Krinner, G., Lebas, N., Levavasseur, G., Lévy, C., Li, L., Lott, F., Lurton, T., Luyssaert, S., Madec, G., Madeleine, J.-B., Maignan, F., Marchand, M., Marti, O., Mellul, L., Meurdesoif, Y., Mignot, J., Musat, I., Ottlé, C., Peylin, P., Planton, Y., Polcher, J., Rio, C., Rochetin, N., Rousset, C., Sepulchre, P., Sima, A., Swingedouw, D., Thiéblemont, R., Traore, A.K., Vancoppenolle, M., Vial, J., Vialard, J., Viovy, N., Vuichard, N., 2020. Presentation and Evaluation of the IPSL-CM6A-LR Climate Model. Journal of Advances in Modeling Earth Systems 12, e2019MS002010. https://doi.org/10.1029/2019MS002010

Cannon, A.J., Sobie, S.R., Murdock, T.Q., 2015. Bias Correction of GCM Precipitation by Quantile Mapping: How Well Do Methods Preserve Changes in Quantiles and Extremes? Journal of Climate 28, 6938–6959. https://doi.org/10.1175/JCLI-D-14-00754.1

Court, A., 1958. Review of Some Applications of Statistics to Meteorology. Bulletin of the American Meteorological Society 39, 502–503.

Cuffey, K.M., Paterson, W.S.B., 2010. The Physics of Glaciers. Academic Press.

Eyring, V., Mishra, V., Griffith, G.P., Chen, L., Keenan, T., Turetsky, M.R., Brown, S., Jotzo, F., Moore, F.C., van der Linden, S., 2021. Reflections and projections on a decade of climate science. Nat. Clim. Chang. 11, 279–285. https://doi.org/10.1038/s41558-021-01020-x

Gagliardini, O., Zwinger, T., Gillet-Chaulet, F., Durand, G., Favier, L., de Fleurian, B., Greve, R., Malinen, M., Martín, C., Råback, P., Ruokolainen, J., Sacchettini, M., Schäfer, M., Seddik, H., Thies, J., 2013. Capabilities and performance of Elmer/Ice, a new-generation ice sheet model. Geoscientific Model Development 6, 1299–1318. https://doi.org/10.5194/gmd-6-1299-2013

Gilbert, A., Sinisalo, A., Gurung, T.R., Fujita, K., Maharjan, S.B., Sherpa, T.C., Fukuda, T., 2020. The influence of water percolation through crevasses on the thermal

regime of a Himalayan mountain glacier. The Cryosphere 14, 1273–1288. https://doi.org/10.5194/tc-14-1273-2020

Gillett, N.P., Kirchmeier-Young, M., Ribes, A., Shiogama, H., Hegerl, G.C., Knutti, R., Gastineau, G., John, J.G., Li, L., Nazarenko, L., Rosenbloom, N., Seland, Ø., Wu, T., Yukimoto, S., Ziehn, T., 2021. Constraining human contributions to observed warming since the pre-industrial period. Nat. Clim. Chang. 11, 207–212. https://doi.org/10.1038/s41558-020-00965-9

Gillett, N.P., Shiogama, H., Funke, B., Hegerl, G., Knutti, R., Matthes, K., Santer, B.D., Stone, D., Tebaldi, C., 2016. The Detection and Attribution Model Intercomparison Project (DAMIP v1.0) contribution to CMIP6. Geoscientific Model Development 9, 3685–3697. https://doi.org/10.5194/gmd-9-3685-2016

Gimbert, F., Gilbert, A., Gagliardini, O., Vincent, C., Moreau, L., 2021. Do Existing Theories Explain Seasonal to Multi-Decadal Changes in Glacier Basal Sliding Speed? Geophysical Research Letters 48, e2021GL092858. https://doi.org/10.1029/2021GL092858

Gutiérrez, J.M., Maraun, D., Widmann, M., Huth, R., Hertig, E., Benestad, R., Roessler, O., Wibig, J., Wilcke, R., Kotlarski, S., San Martín, D., Herrera, S., Bedia, J., Casanueva, A., Manzanas, R., Iturbide, M., Vrac, M., Dubrovsky, M., Ribalaygua, J., Pórtoles, J., Räty, O., Räisänen, J., Hingray, B., Raynaud, D., Casado, M.J., Ramos, P., Zerenner, T., Turco, M., Bosshard, T., Štěpánek, P., Bartholy, J., Pongracz, R., Keller, D.E., Fischer, A.M., Cardoso, R.M., Soares, P.M.M., Czernecki, B., Pagé, C., 2019. An intercomparison of a large ensemble of statistical downscaling methods over Europe: Results from the VALUE perfect predictor cross-validation experiment. International Journal of Climatology 39, 3750–3785. https://doi.org/10.1002/joc.5462

Haustein, K., Allen, M.R., Forster, P.M., Otto, F.E.L., Mitchell, D.M., Matthews, H.D., Frame, D.J., 2017. A real-time Global Warming Index. Sci Rep 7, 15417. https://doi.org/10.1038/s41598-017-14828-5

Hawkins, E., Ortega, P., Suckling, E., Schurer, A., Hegerl, G., Jones, P., Joshi, M., Osborn, T.J., Masson-Delmotte, V., Mignot, J., Thorne, P., Oldenborgh, G.J. van, 2017. Estimating Changes in Global Temperature since the Preindustrial Period. Bulletin of the American Meteorological Society 98, 1841–1856. https://doi.org/10.1175/BAMS-D-16-0007.1

Hawkins, E., Sutton, R., 2012. Time of emergence of climate signals. Geophysical Research Letters 39. https://doi.org/10.1029/2011GL050087

Hock, R., 1999. A distributed temperature-index ice- and snowmelt model including potential direct solar radiation. Journal of Glaciology 45, 101–111. https://doi.org/10.3189/S0022143000003087

Huss, M., Hock, R., 2015. A new model for global glacier change and sea-level rise. Frontiers in Earth Science 3.

Jiang, W., Gastineau, G., Codron, F., 2021. Multicentennial Variability Driven by Salinity Exchanges Between the Atlantic and the Arctic Ocean in a Coupled Climate Model. Journal of Advances in Modeling Earth Systems 13, e2020MS002366. https://doi.org/10.1029/2020MS002366

Kaser, G., Großhauser, M., Marzeion, B., 2010. Contribution potential of glaciers to water availability in different climate regimes. Proceedings of the National Academy of Sciences 107, 20223–20227. https://doi.org/10.1073/pnas.1008162107

Latombe, G., Burke, A., Vrac, M., Levavasseur, G., Dumas, C., Kageyama, M., Ramstein, G., 2018. Comparison of spatial downscaling methods of general circulation model results to study climate variability during the Last Glacial Maximum. Geoscientific Model Development 11, 2563–2579. https://doi.org/10.5194/gmd-11-2563-2018

Laurent, L., Buoncristiani, J.-F., Pohl, B., Zekollari, H., Farinotti, D., Huss, M., Mugnier, J.-L., Pergaud, J., 2020. The impact of climate change and glacier mass loss on the hydrology in the Mont-Blanc massif. Sci Rep 10, 10420. https://doi.org/10.1038/s41598-020-67379-7

Leclercq, P.W., Oerlemans, J., Basagic, H.J., Bushueva, I., Cook, A.J., Le Bris, R., 2014. A data set of worldwide glacier length fluctuations. The Cryosphere 8, 659–672. https://doi.org/10.5194/tc-8-659-2014

Li, C., Wang, Z., Zwiers, F., Zhang, X., 2021. Improving the Estimation of Human Climate Influence by Selecting Appropriate Forcing Simulations. Geophysical Research Letters 48, e2021GL095500. https://doi.org/10.1029/2021GL095500

Luo, M., Liu, T., Meng, F., Duan, Y., Frankl, A., Bao, A., De Maeyer, P., 2018. Comparing Bias Correction Methods Used in Downscaling Precipitation and Temperature from Regional Climate Models: A Case Study from the Kaidu River Basin in Western China. Water 10, 1046. https://doi.org/10.3390/w10081046

Mann, M.E., Zhang, Z., Rutherford, S., Bradley, R.S., Hughes, M.K., Shindell, D., Ammann, C., Faluvegi, G., Ni, F., 2009. Global Signatures and Dynamical Origins of the Little Ice Age and Medieval Climate Anomaly. Science 326, 1256–1260. https://doi.org/10.1126/science.1177303

Marzeion, B., Cogley, J.G., Richter, K., Parkes, D., 2014. Attribution of global glacier mass loss to anthropogenic and natural causes. Science 345, 919–921.

Marzeion, B., Hock, R., Anderson, B., Bliss, A., Champollion, N., Fujita, K., Huss, M., Immerzeel, W.W., Kraaijenbrink, P., Malles, J.-H., Maussion, F., Radić, V., Rounce, D.R., Sakai, A., Shannon, S., van de Wal, R., Zekollari, H., 2020. Partitioning the Uncertainty of Ensemble Projections of Global Glacier Mass Change. Earth's Future 8, e2019EF001470. https://doi.org/10.1029/2019EF001470

Maussion, F., Butenko, A., Champollion, N., Dusch, M., Eis, J., Fourteau, K., Gregor, P., Jarosch, A.H., Landmann, J., Oesterle, F., Recinos, B., Rothenpieler, T., Vlug, A., Wild, C.T., Marzeion, B., 2019. The Open Global Glacier Model (OGGM) v1.1.

Geoscientific Model Development 12, 909–931. https://doi.org/10.5194/gmd-12-909-2019

Milner, A.M., Khamis, K., Battin, T.J., Brittain, J.E., Barrand, N.E., Füreder, L., Cauvy-Fraunié, S., Gíslason, G.M., Jacobsen, D., Hannah, D.M., Hodson, A.J., Hood, E., Lencioni, V., Ólafsson, J.S., Robinson, C.T., Tranter, M., Brown, L.E., 2017. Glacier shrinkage driving global changes in downstream systems. Proceedings of the National Academy of Sciences 114, 9770–9778. https://doi.org/10.1073/pnas.1619807114

Myhre, G., Forster, P.M., Samset, B.H., Hodnebrog, Ø., Sillmann, J., Aalbergsjø, S.G., Andrews, T., Boucher, O., Faluvegi, G., Fläschner, D., Iversen, T., Kasoar, M., Kharin, V., Kirkevåg, A., Lamarque, J.-F., Olivié, D., Richardson, T.B., Shindell, D., Shine, K.P., Stjern, C.W., Takemura, T., Voulgarakis, A., Zwiers, F., 2017. PDRMIP: A Precipitation Driver and Response Model Intercomparison Project—Protocol and Preliminary Results. Bulletin of the American Meteorological Society 98, 1185–1198. https://doi.org/10.1175/BAMS-D-16-0019.1

Oerlemans, J., 2001. Glaciers and Climate Change. CRC Press.

Painter, T.H., Flanner, M.G., Kaser, G., Marzeion, B., VanCuren, R.A., Abdalati, W., 2013. End of the Little Ice Age in the Alps forced by industrial black carbon. Proc. Natl. Acad. Sci. U.S.A. 110, 15216–15221. https://doi.org/10.1073/pnas.1302570110

Panofsky, H. A., & Brier, G. W. (1968). *Some applications of statistics to meteorology*. Earth and Mineral Sciences Continuing Education, College of Earth and Mineral Sciences

Parsons, L.A., Brennan, M.K., Wills, R.C.J., Proistosescu, C., 2020. Magnitudes and Spatial Patterns of Interdecadal Temperature Variability in CMIP6. Geophysical Research Letters 47, e2019GL086588. https://doi.org/10.1029/2019GL086588

Piani, C., Haerter, J.O., 2012. Two dimensional bias correction of temperature and precipitation copulas in climate models. Geophysical Research Letters 39. https://doi.org/10.1029/2012GL053839

Protin, M., Schimmelpfennig, I., Mugnier, J.-L., Ravanel, L., Le Roy, M., Deline, P., Favier, V., Buoncristiani, J.-F., Aumaître, G., Bourlès, D.L., Keddadouche, K., 2019. Climatic reconstruction for the Younger Dryas/Early Holocene transition and the Little Ice Age based on paleo-extents of Argentière glacier (French Alps). Quaternary Science Reviews 221, 105863. https://doi.org/10.1016/j.quascirev.2019.105863

Rabatel, A., Sanchez, O., Vincent, C., Six, D., 2018. Estimation of Glacier Thickness From Surface Mass Balance and Ice Flow Velocities: A Case Study on Argentière Glacier, France. Frontiers in Earth Science 6.

Reveillet, M., Dumont, M., Gascoin, S., Lafaysse, M., Nabat, P., Ribes, A., Nheili, R., Tuzet, F., Menegoz, M., Morin, S., Picard, G., Ginoux, P., 2021. Black carbon and

584 dust alter the response of mountain snowcover under climate change (preprint). In
585 Review. https://doi.org/10.21203/rs.3.rs-800501/v1
586 Ribes, A., Qasmi, S., Gillett, N., 2021. Updated attribution of GSAT changes and
587 implications EGU21-16112. https://doi.org/10.5194/egusphere-egu21-16112
588 Roe, G.H., Baker, M.B., Herla, F., 2017. Centennial glacier retreat as categorical
589 evidence of regional climate change. Nature Geosci 10, 95–99.
590 https://doi.org/10.1038/ngeo2863
591 Roe, G.H., Christian, J.E., Marzeion, B., 2021. On the attribution of industrial-era glacier
592 mass loss to anthropogenic climate change. The Cryosphere 15, 1889–1905.
593 https://doi.org/10.5194/tc-15-1889-2021
594 Six, D., Vincent, C., 2014. Sensitivity of mass balance and equilibrium-line altitude to
595 climate change in the French Alps. J. Glaciol. 60, 867–878.
596 https://doi.org/10.3189/2014JoG14J014
597 Vaittinada Ayar, P., Vrac, M., Mailhot, A., 2021. Ensemble bias correction of climate
598 simulations: preserving internal variability. Sci Rep 11, 3098.
599 https://doi.org/10.1038/s41598-021-82715-1
600 Vernay, M., Lafaysse, M., Monteiro, D., Hagenmuller, P., Nheili, R., Samacoïts, R.,
601 Verfaillie, D., Morin, S., 2022. The S2M meteorological and snow cover reanalysis
602 over the French mountainous areas: description and evaluation (1958–2021). Earth
603 System Science Data 14, 1707–1733. https://doi.org/10.5194/essd-14-1707-2022
604 Vincent, C., Le Meur, E., Six, D., Funk, M., 2005. Solving the paradox of the end of the
605 Little Ice Age in the Alps. Geophysical Research Letters 32.
606 https://doi.org/10.1029/2005GL022552
607 Vincent, C., Peyaud, V., Laarman, O., Six, D., Gilbert, A., Gillet-Chaulet, F., Berthier, E.,
608 Morin, S., Verfaillie, D., Rabatel, A., Jourdain, B., Bolibar, J., 2019. Déclin des deux
609 plus grands glaciers des Alpes françaises au cours du XXI e siècle : Argentière et
610 Mer de Glace. La Météorologie.
611 Vincent, C., Soruco, A., Six, D., Meur, E.L., 2009. Glacier thickening and decay analysis
612 from 50 years of glaciological observations performed on Glacier d'Argentière, Mont
613 Blanc area, France. Annals of Glaciology 50, 73–79.
614 https://doi.org/10.3189/172756409787769500
615 Weertman, J., 1957. On the Sliding of Glaciers. Journal of Glaciology 3, 33–38.
616 https://doi.org/10.3189/S0022143000024709
617